

# Spatial structure of the HIRLAM mean-sea-level pressure forecast error

By SIMO JÄRVENOJA, Finnish Meteorological Institute

25th February 2005

## 1 Introduction

Surface pressure ( $p_s$ ) is a model variable that can capture model errors or deficiencies due to various parametrized processes and the dynamics. This study deals with mean-sea-level pressure ( $p_{msl}$ ), a close relative to surface pressure, and its forecast error. The  $p_{msl}$  forecast error is defined here as the difference between the forecast and the verifying analysis of  $p_{msl}$ .

Monthly maps of geographical distribution of  $p_{msl}$  forecast errors, systematic error (or bias) and root-mean-square error (rms error), are produced at NWP centers, e.g., at FMI, in routine verification procedures. The forecast error patterns show seasonal differences in the magnitude, with larger errors in synoptically active seasons, in fall and winter, than in summer. On the other hand, the error structures differ largely from month to month, thus indicating dependence on the general flow type.

## 2 Data

The operational HIRLAM at FMI started in January 1990. Field verification of the forecasts has been carried out since June 1990 and the resulting verification data have been archived. This archive makes it possible to study the model performance, e.g., the  $p_{msl}$  bias structure and its temporal changes.

The operational FMI HIRLAM has been run in different areas and in different resolutions. A period from September 1996 to February 2004 has been selected for the present study because the model domain has been almost the same. Monthly  $p_{msl}$  bias fields of 48 h forecasts together with analysed monthly  $p_{msl}$  mean fields from this period are the input data for the present study. These monthly bias fields as well as mean fields are based on all four daily cycles. The above mentioned period can be divided into three different parts, depending on 1) the model version and 2) geographical model area, as follows.

- LOU : September 1996 - November 1997 ; NSF model,  $194 \times 140$ ,  $0.4^\circ$   
December 1997 - October 1999 ; ATL model,  $194 \times 140$ ,  $0.4^\circ$
- CBR : October 1999 - May 2003 ; ATA model,  $194 \times 140$ ,  $0.4^\circ$
- CBN : March 2003 - February 2004 ; ATX model,  $256 \times 186$ ,  $0.3^\circ$

The data for the period September 1996 to February 2004 are thus divided into three sub-periods called "LOU", "CBR" and "CBN", with the naming representing the turbulence scheme used in each period (explained later in more detail). The operational HIRLAM version of the LOU period (September 1996 - October 1999) was based on version 2.5 with some updates picked from later releases. Two production versions, NSF and ATL, were run during the LOU period, basically differing in terms of the parallelization method. NSF was run on the Cray C94 with autotasking parallelization, whereas ATL was the first model version developed for an MPP computer, Cray T3E, with SHMEM libraries used for parallelization. The model domain (seen in Fig. 1) consisted of  $194 \times 140$  grid points with the horizontal resolution being  $0.4^\circ$ . The number of model levels in the vertical was 31. The name (LOU) comes from the turbulence scheme used, i.e., the Louis scheme. The HIRLAM system (production name ATA) of the second period (CBR, October 1999 - May 2003) was based on version 4.6.2, and the name comes from the CBR turbulence scheme. The model domain, number of grid points and vertical levels as well as the horizontal resolution are the same as those of LOU. The HIRLAM system (ATX) of the third period (CBN, March 2003 - February 2004) was based on version 5.1.4. The model domain (seen in Fig. 5), slightly smaller than that of LOU and CBR, consisted of  $256 \times 186$  grid points with the horizontal resolution being  $0.3^\circ$ . The number of levels in the vertical was 40. The turbulence scheme of the CBN period was a modified version from that of CBR. Monthly  $p_{msl}$  bias fields from these three periods of LOU (38 cases), CBR (44 cases) and CBN (13 cases) are then used in further calculations.

In addition to monthly mean data, daily  $p_{msl}$  forecasts and analyses (based on 00 UTC) and calculated forecast error fields for the period December 2002 to May 2003 are used. Data from two HIRLAM systems, CBR and CBN, are available.

### 3 Bias of $p_{msl}$

#### 3.1 Examples of monthly bias

The  $p_{msl}$  bias can vary rather much from month to month, depending on the general flow type. In general, bias is smaller in summertime when the flow is weak, and larger in autumn and winter in presence of a stronger flow. Figures 1 and 2 give two examples of different types of biases. Figure 1 shows the (48 h)  $p_{msl}$  bias together with the average  $p_{msl}$  pattern for a summer month, July 1999. This is an example of "a quiet summer month", when the flow is weak. Consequently, the bias values are also small, with positive bias of the order 2 hPa seen in the western part of the area over northern America, and negative bias of -3 hPa over Greenland and a small negative bias also close to the eastern boundary. Bias values are small elsewhere. Figure 2, on the other hand, is an example of "an active cyclone month", when a low pressure area dominated over northern Europe and the Arctic Sea north of Scandinavia. Again, there is a positive bias in the western part of the model domain as well as close to the northern boundary. The whole central and northern Europe as well as Russia are dominated by a large-scale negative bias, reaching 5 hPa over the Baltic states and further in the east over Russia. These two maps are examples of extreme cases, usually the bias varies between these values.

## 3.2 Long-term bias

Figures 3-5 demonstrate the geographical distribution of the (48 h)  $p_{msl}$  bias for three different periods of LOU, CBR and CBN, respectively. The averaging period varies from about one year (CBN) to almost four years (CBR). Therefore, it should be kept in mind that Figs. 3-5 represent annual mean biases, and the magnitude of the bias shown is smaller than it is in active seasons (autumn and winter) but larger than in summer.

Figure 3, showing the  $p_{msl}$  bias for the LOU period, indicates that a positive bias of the order of 1 hPa (or locally more) dominates in the northwestern corner of the model domain and also over the Mediterranean. On the other hand, a negative bias of about 1 hPa is seen over Europe and Russia. The bias distribution of the CBR period (Fig. 4) much resembles that of LOU. Again, a positive bias appears in the vicinity of the western boundary and over the Mediterranean, but some positive bias is seen also over northern Europe and over the Arctic Sea. The area of the negative bias over Europe is significantly smaller than that in LOU and is located around the Black Sea. Figure 5 demonstrates the bias distribution for the CBN period. It can be seen that the positive bias in the western part of the area is clearly smaller than that in LOU and CBR. A similar positive bias as in LOU and CBR is seen in the Mediterranean area. A negative bias, more than 1.5 hPa at most, covers large parts of Europe and Russia as well as areas around Greenland. The negative bias over Europe and Russia is largest in CBN.

A general feature in the  $p_{msl}$  bias for all periods (LOU, CBR, CBN) is a positive bias close to the western boundary - the inflow boundary, and a negative bias over Europe and Russia close to the eastern boundary - the outflow boundary. The magnitude of the bias, however, differs from period to period.

The negative bias over Europe and Russia is most probably, at least partly, generated by the HIRLAM model's inability to fill the occluding cyclones, as can be deduced from Fig. 2, for example. There seems to be a connection to the turbulence scheme used: the Louis scheme (LOU) and the enhanced CBR scheme (of 5.1.4) used in the CBN period result in larger negative bias over Europe and Russia than the 4.6.2 version in the CBR period.

Finally, Fig. 6 depicts the  $p_{msl}$  bias in 48 h ECMWF forecasts (from 12 UTC analyses only) for 1998-2003. The magnitude of the bias is generally small, exceeding  $\pm 1$  hPa only over Canada and around the Black Sea/Caspian Sea area, and does not grow much as a function of the forecast length (up to 10 days). The distribution is such that a positive bias dominates over northern America, over the Arctic Sea north of Europe and over the Pacific. The negative bias is seen over Eastern Europe and Eurasia as well as in the Middle East. In this respect the ECMWF bias is similar to that of HIRLAM. It could, therefore, be possible that ECMWF forecasts used as lateral boundary conditions for the HIRLAM forecasts, at least partly, contribute to the  $p_{msl}$  bias pattern of HIRLAM.

## 4 EOF analysis

Empirical orthogonal function (EOF) analysis is applied to monthly bias fields and daily forecast error fields. The EOFs are found as eigenvectors of the temporal covariance matrix (e.g., Rinne and Karhila, 1979; Rinne and Järvenoja, 1979) computed between bias (forecast error) fields. Thus any bias (forecast error) field can be represented by

$$e(i, t) = em(i) + \sum_{\nu=1}^N C_{\nu}(t)f_{\nu}(i), \quad (1)$$

where  $e(i, t)$  is the bias (or forecast error), with  $i$  and  $t$  referring to space (grid point) and time, respectively. Term  $em(i)$  represents the sample mean of  $e$  at each grid point. The sum term consists of the space-dependent part  $f_{\nu}$ , the spatial EOF pattern and the time-dependent coefficient  $C_{\nu}$ , for component  $\nu$ . Value  $N$  represents the point of truncation, number of terms taken to the EOF series. The EOFs have such a property that the low-indexed components ( $f_{\nu}$  with  $\nu$  being small) represent largest horizontal scales.

In the present study, the EOFs have been computed from full fields of  $p_{msl}$  bias, i.e., the sample mean has not been subtracted from each monthly bias field ( $em(i) = 0$ ). The EOFs have been determined separately from monthly biases for different periods (LOU, CBR and CBN) as well as from daily forecast errors for CBR and CBN (December 2002 - May 2003).

#### 4.1 Monthly EOF

Figures 7 and 8 demonstrate the two leading EOF patterns (EOF-1 or  $f_1$  and EOF-2 or  $f_2$ ) of the monthly  $p_{msl}$  bias for the LOU period. The EOF patterns are scaled so that the area average of the squared grid point values equals unity (1). EOF-1 (Fig. 7) bears a high resemblance to the average bias field of the LOU period (Fig. 3). The negative values of EOF-1 over Europe and Russia coincide with the negative bias values (Fig. 3). Similarly, the positive values of EOF-1 in the western and northern part of the model domain correspond to the positive bias values. The first EOF is clearly the most dominant EOF (of all 38 possible) and it explains 47 % of the total monthly forecast error variance. As EOF-1 clearly resembles the long-term average bias field, it can be therefore concluded that almost half of the monthly forecast error is due to the systematic error. The time-dependent coefficient  $C_1$  of EOF-1 ( $f_1$ ) is always positive, but is varying from month to month (will be discussed later in more detail). Figure 8 shows the spatial pattern of EOF-2. EOF-2 has negative values over northern Europe and Russia as well as in the western part of the model domain. Positive values are seen only over Greenland. EOF-2 accounts for 10 % of the total monthly forecast error variance.

Figures 9 and 10 depict the two leading EOF patterns for the CBR period. EOF-1 (Fig. 9) has similarities to EOF-1 of the LOU period (Fig. 7), but the negative cell over Europe is smaller than that of the LOU period. Again, the EOF-1 pattern resembles much the corresponding sample mean error (Fig. 4). EOF-1 explains 49 % of the total monthly forecast error variance. EOF-2 (Fig. 10) is different from EOF-2 of the LOU period (Fig. 8), but still shows a negative cell over eastern Europe and Russia. EOF-2 explains 8 % of the total forecast error variance.

The two leading EOF patterns for the CBN period resemble those of the LOU period (not shown).

Figure 11 demonstrates the time-dependent coefficients,  $C_1$  and  $C_2$ , of the two leading EOFs ( $f_1$  and  $f_2$ ) for the period September 1996 to May 2003. Note that coefficients  $C_1$  and  $C_2$  are based for two separate periods (LOU and CBR) and thus for different sets of EOFs.

Coefficient  $C_1$  is always positive, but it is varying from month to month. This means that EOF-1 always tends to build a negative bias over Europe and Russia, and a positive bias over the western part of model area. The average value of  $C_1$  is about 0.75 hPa, which means that EOF-1 contributes by about 1 hPa ( $C_1 \times f_1$ ) to the negative bias over Europe and Russia on

average. Values of  $C_1$  exceed 1 hPa in some winter months, i.e., EOF-1 contributes more to the negative bias over Europe in wintertime. Coefficient  $C_2$  varies around zero, and has a mean of zero. Again, positive values tend to contribute to the negative bias over Europe (EOF-2 pattern negative over Europe). On the other hand, if the value of  $C_2$  is negative, EOF-2 tends to cancel the negative bias due to EOF-1 over Europe. The positive values of  $C_2$  seem to appear in fall and winter, and thus contribute to the negative bias over Europe in active cyclone months.

The two leading EOFs explain about 60 % of the total monthly forecast error variance. The remaining EOFs (3...38 for LOU, 3...44 for CBR) explain the rest of the error variance (about 40 %) and represent smaller horizontal scales.

## 4.2 Daily EOF

Figure 12 shows an example of an EOF pattern based on daily forecast errors. This leading EOF (EOF-1) is computed from daily 48 h forecast errors (00 UTC forecasts only) for the period December 2002 to May 2003. EOF-1 shows a large negative cell over Europe and Russia. This pattern also resembles the long-term bias pattern of the CBN period (Fig. 5). EOF-1 based on daily forecast errors explains only 15 % of the total forecast error variance (compared to 47/49 % based on monthly errors). This is due to the fact that daily forecast errors can include a larger variety of error structures, which are not present in monthly (filtered) bias fields.

## 4.3 Combined EOF

The EOFs presented in Section 4 are based on a single variable, the  $p_{msl}$  bias (or forecast error). In this section, a method of a combined EOF (CEOF) analysis (Kutzbach, 1967) is applied. Combined EOFs are based on two (or more) variables. A two-variable EOF analysis is used in the following. The variables are the monthly (48 h)  $p_{msl}$  bias (as in Section 4.1) and the monthly  $p_{msl}$  departure from the area average of  $p_{msl}$ , a variable roughly representing the monthly  $p_{msl}$  anomaly. The two parts of data vector, those of the bias and the departure, are scaled with the square root of their respective variances so as to give equal weights for both variables in the CEOF analysis. The CEOF analysis is applied for three different periods (LOU, CBR and CBN), for monthly data only. The idea of this CEOF analysis is to try to find possible connections between the bias structure and the flow type.

In the following, some leading CEOF patterns will be presented. Figures 13 and 14 demonstrate CEOF-1 patterns of the  $p_{msl}$  bias and the  $p_{msl}$  departure, respectively, for the LOU period. Note that CEOF-1 consists of two separate parts, those of the bias and the departure (corresponding to the two parts of the data vector). CEOF-1 of the bias (Fig. 13) corresponds to EOF-1 in Fig. 7, and there is a high resemblance between those. This means that the CEOF analysis is able to reproduce the leading mode in a similar manner as does the EOF analysis of a single variable. The CEOF-1 pattern of the departure (Fig. 14) is shown in a different way compared to that of the bias (Fig 13). First, the actual CEOF-1 pattern of the departure is multiplied by the value of the square root of the variance (eigenvalue) associated to CEOF-1, and then the time-average of  $p_{msl}$  in the model domain is added to that field. As a result, a  $p_{msl}$  field (Fig. 14) corresponding to the actual departure is obtained. In this case, the departure part of CEOF-1 represents a flow type where a large-scale low over the North Atlantic dominates. As the time-dependent coefficient associated with CEOF-1 is always positive, it means that CEOF-1 tends to build a negative bias over Europe and tends to maintain a low pressure area

over the Atlantic. The magnitude of the time-dependent coefficient varies from month to month, and consequently, the magnitude of the bias and the intensity of the low pressure as well. The type of a flow pattern shown in Fig. 14 is typical of winter conditions, and has been frequent in the 1990's, during the positive phase of the North Atlantic Oscillation (NAO). The CEOF analysis suggests that the bias structure during the LOU period (Figs. 7 and 13) is related to the flow type of Fig. 14. CEOF-1 is very dominant as it accounts for 44 % of the total variance.

The bias parts of CEOF-1 for CBR and CBN periods resemble those of the corresponding EOF-1 patterns of the  $p_{msl}$  bias (not shown). The departure parts of CEOF-1 for CBR and CBN periods (not shown) are highly similar to that of Fig. 14.

Figures 15 and 16 demonstrate CEOF-4 of the bias and departure part, respectively, for the LOU period. This CEOF explains 4 % of the total variance. The striking feature in this pair of figures is the coincidence of the bias structure (Fig. 15) with the low pressure system over the Atlantic west of the British Isles (Fig. 16). This pair of figures strongly supports the impression that low pressure systems were too deep during the era of the Louis turbulence scheme in HIRLAM. As the time-dependent coefficient associated with CEOF-4 can also be negative, Figs. 15 and 16 can therefore be interpreted also so that a positive bias is associated with high pressure areas.

Figures 17 and 18, showing CEOF-5 of the bias and the departure, respectively, for the CBR period, tell a different story. Here the positive bias (Fig. 17) is associated to the low pressure system around the British Isles (Fig. 18). This means that during the CBR period the predicted low pressures were not deep enough, which is clearly confirmed by the field verification results at FMI. In this respect, the Louis turbulence scheme and CBR scheme of the HIRLAM version 4.6.2 behaved differently. The newer CBR version of HIRLAM 5.1.4 (CBN period), however, has the same property of the Louis scheme resulting in too deep cyclones (not shown).

The use of combined EOF analysis has shown that it is possible to relate the observed bias (or forecast error) structure to certain flow types.

## 5 Bias and boundary ?

Section 3.2 described the long-term  $p_{msl}$  bias structure for different periods. A typical feature for all periods was a positive bias close to the western boundary - the inflow boundary, and a negative bias close to eastern boundary - the outflow boundary. As the bias in the ECMWF forecasts used as lateral boundary conditions in HIRLAM shows a similar geographical distribution (positive over northern America, negative over eastern Europe and Eurasia), it could be therefore possible that the HIRLAM  $p_{msl}$  bias is, at least partly, generated by the boundary conditions.

Figures 19 and 20, demonstrating the  $p_{msl}$  bias in 48 h forecasts for February 2004 for the ATX suite (old FMI operational model) and the RCR suite, respectively, reveal a possible connection between the negative bias and the outflow boundary. Both ATX (Fig. 19) and RCR (Fig. 20) have a substantial (more than 3 hPa) negative bias over Europe around 30°E. But RCR, extending further to the east, has an additional negative bias cell of about 3 hPa north of the Caspian Sea close to the eastern boundary. The negative bias around 30°E can be thought to come from the HIRLAM model's inability to fill the occluding cyclones, most likely due to deficiencies in the turbulence scheme. But, can the additional negative cell close to the eastern boundary be related to handling of the lateral boundary values, i.e., deficiencies in the boundary relaxation scheme? Therefore, one could wonder, whether a negative bias cell would still appear

close to the eastern boundary, even if the eastern boundary were placed as far in the east as in India! This could be verified with a set of experiments, in which the eastern boundary is placed at a different location from one experiment to another.

## 6 Summary

The systematic error of HIRLAM  $p_{msl}$  forecasts has been studied. The emphasis of the study has been in analyzing the monthly bias structures, but also daily forecast errors have been dealt with. The EOF analysis has been utilized in this analyzing process.

The study reveals that the monthly bias values are larger in winter than in summer, indicating a dependence on the strength of the mean flow. Generally, the  $p_{msl}$  bias seems to favour a geographical pattern, which shows negative bias values over Europe and Russia and positive values close to the western and northern boundaries. This bias distribution means that a positive bias is frequent close to the western, in-flow boundary, and a negative bias close to the eastern, out-flow boundary. Therefore, one could think that boundaries might in some way be responsible for this type of bias distribution. One candidate for the frequent negative bias over Europe is the well-known HIRLAM model's inability to fill occluding cyclones.

The bias structure and magnitude varies temporally, and seems to be related to the turbulence scheme used in the model. The Louis scheme and later versions of the CBR scheme (e.g., version 5.1.4) tended to lead to bias patterns where a negative bias was related to low pressure areas, whereas an earlier CBR version (4.6.2) behaved differently, by resulting in a positive bias connected with lows.

The EOF analysis has been widely used in the present study. This analysis shows, for example, that the most important mode (EOF-1) computed from monthly bias fields much resembles the pattern of the long-term bias field. Therefore, EOF-1 can be related to the long-term bias of the forecast error. As EOF-1 explains almost half of the monthly forecast error variance, bias seems to be really dominant in the monthly time scale of the forecast error. The combined EOF analysis shows that it is possible to relate observed bias patterns to certain flow types.

## Acknowledgement

Prof. Emer. Juhani Rinne is acknowledged for his valuable comments.

## References

- Kutzbach, J.E., 1967: Empirical eigenvectors of sea-level pressure, surface temperature and precipitation complexes over North America. *J. Appl. Meteor.*, **6**, 791-802.
- Rinne, J. and V. Karhila, 1979: Empirical orthogonal functions of 500 mb height in the northern hemisphere determined from a large data sample. *Quart. J. Roy. Met. Soc.*, **105**, 873-884.
- Rinne, J. and S. Järvenoja, 1979: Truncation of the EOF series representing 500 mb heights. *Quart. J. Roy. Met. Soc.*, **105**, 885-897.

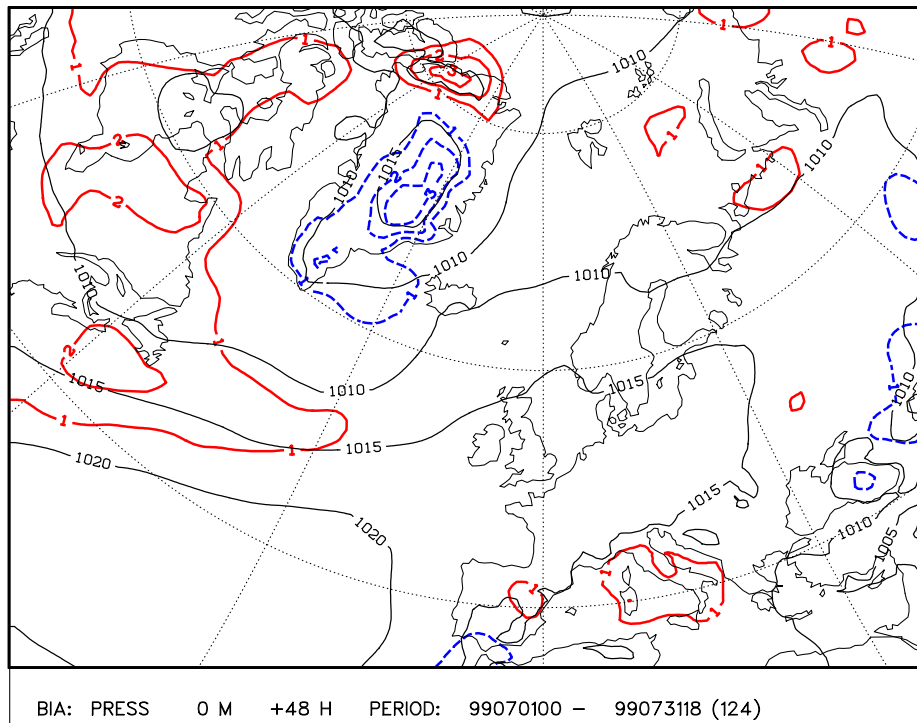


Figure 1: Average  $p_{msl}$  together with the  $p_{msl}$  bias in 48 h forecasts for July 1999, for "a quiet summer month". Average  $p_{msl}$  is indicated with thin lines, with a contour interval of 5 hPa. Bias of  $p_{msl}$  is indicated with thicker lines, with a contour interval of 1 hPa; the zero isoline not plotted, negative values indicated with dashed lines.

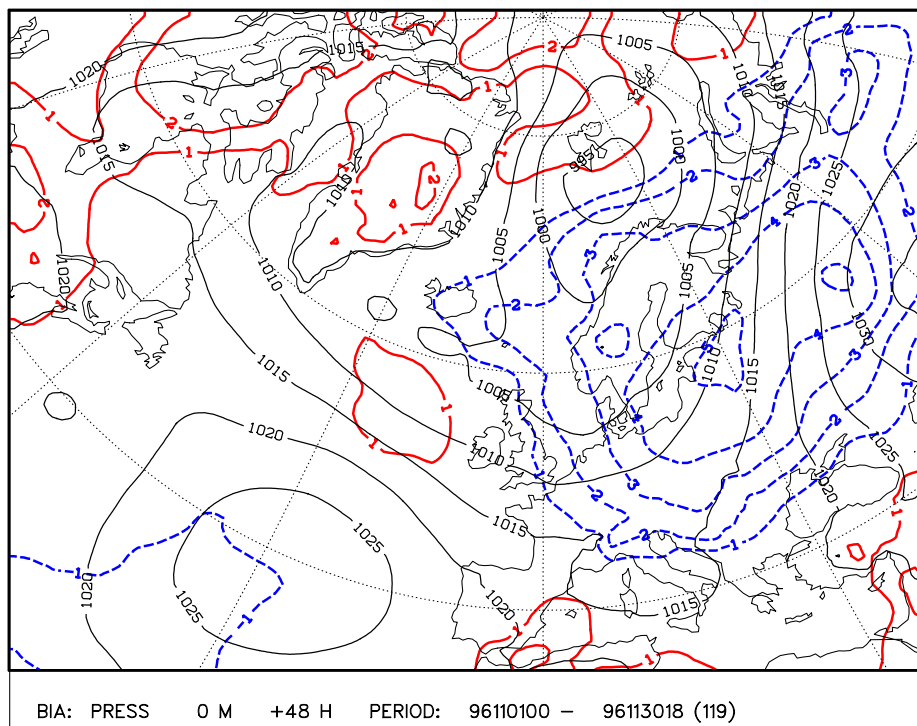


Figure 2: Average  $p_{msl}$  together with the  $p_{msl}$  bias in 48 h forecasts for November 1996, for "an active cyclone month". Contours as in Fig. 1.

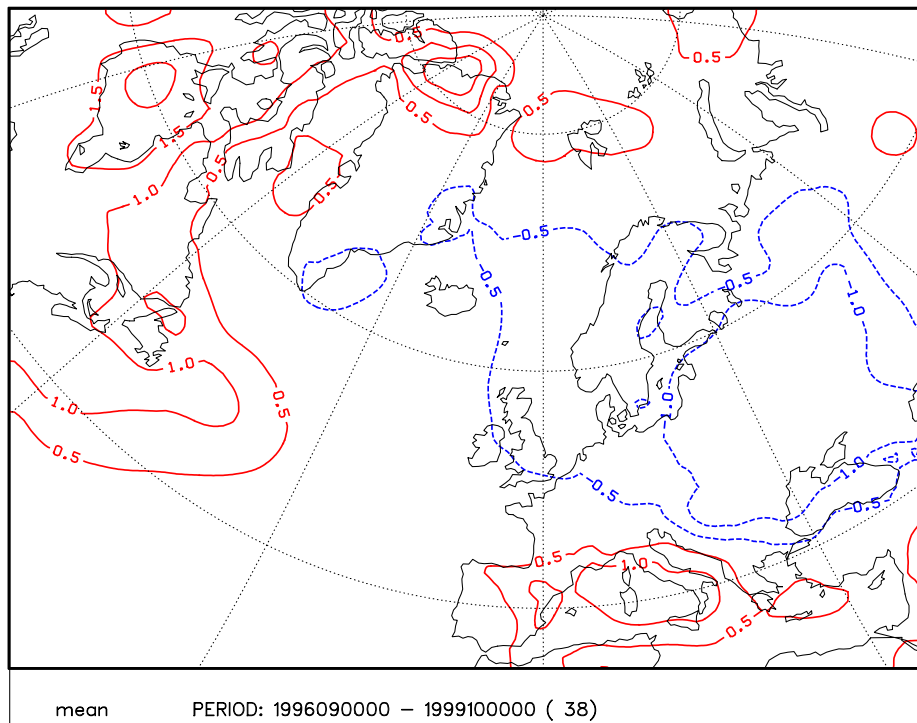


Figure 3: Systematic forecast error (bias) of  $p_{msl}$  in 48 h "LOU" forecasts, for September 1996 - October 1999. Contour interval: 0.5 hPa. The zero isoline not plotted, negative values indicated with dashed lines.

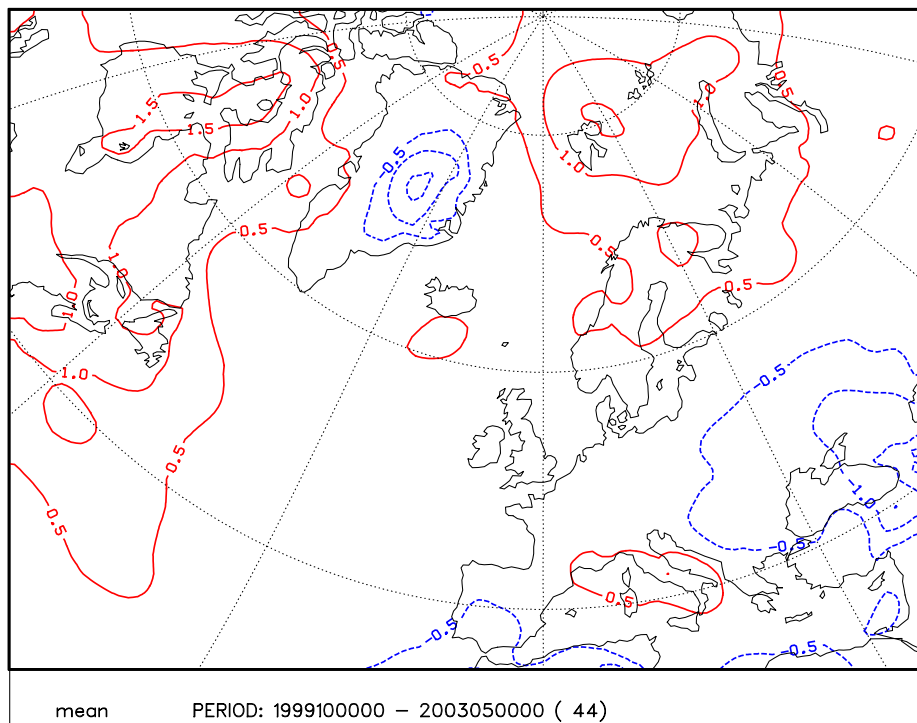


Figure 4: Systematic forecast error (bias) of  $p_{msl}$  in 48 h "CBR" forecasts, for October 1999 - May 2003. Contour interval: 0.5 hPa. The zero isoline not plotted, negative values indicated with dashed lines.

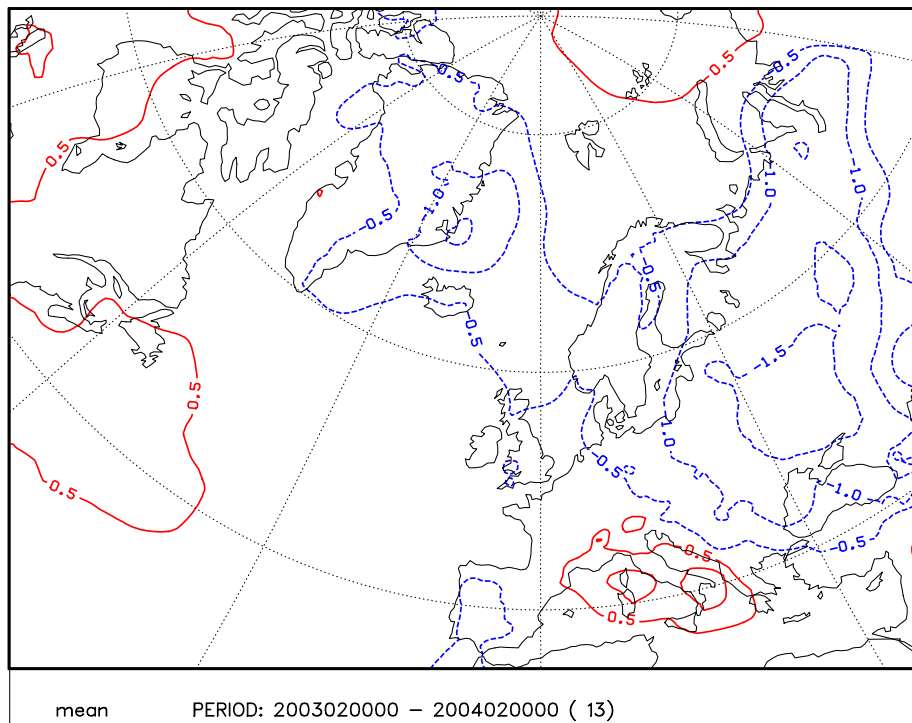


Figure 5: *Systematic forecast error (bias) of  $p_{msl}$  in 48 h "CBN" forecasts, for February 2003 - February 2004. Contour interval: 0.5 hPa. The zero isoline not plotted, negative values indicated with dashed lines.*

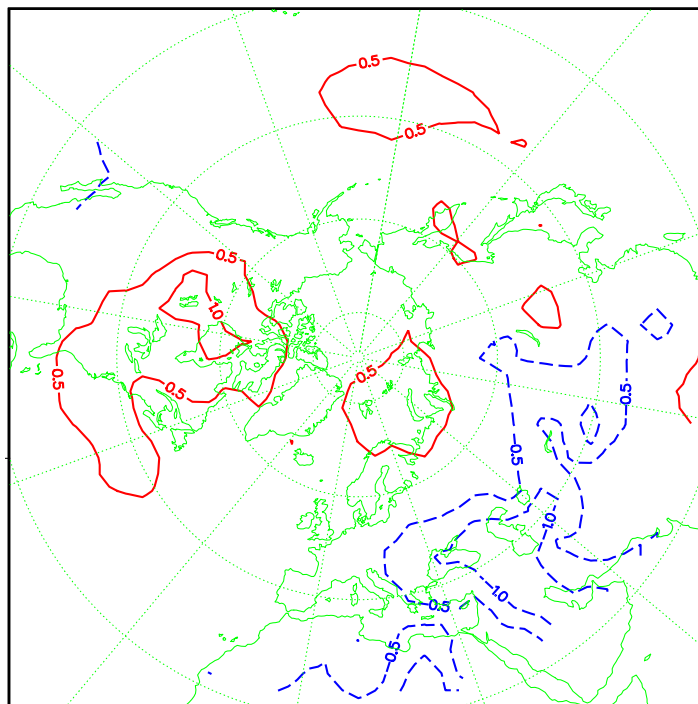


Figure 6: *Systematic forecast error (bias) of  $p_{msl}$  in 48 h ECMWF forecasts, for 1998 - 2003. Contour interval: 0.5 hPa. The zero isoline not plotted, negative values indicated with dashed lines.*

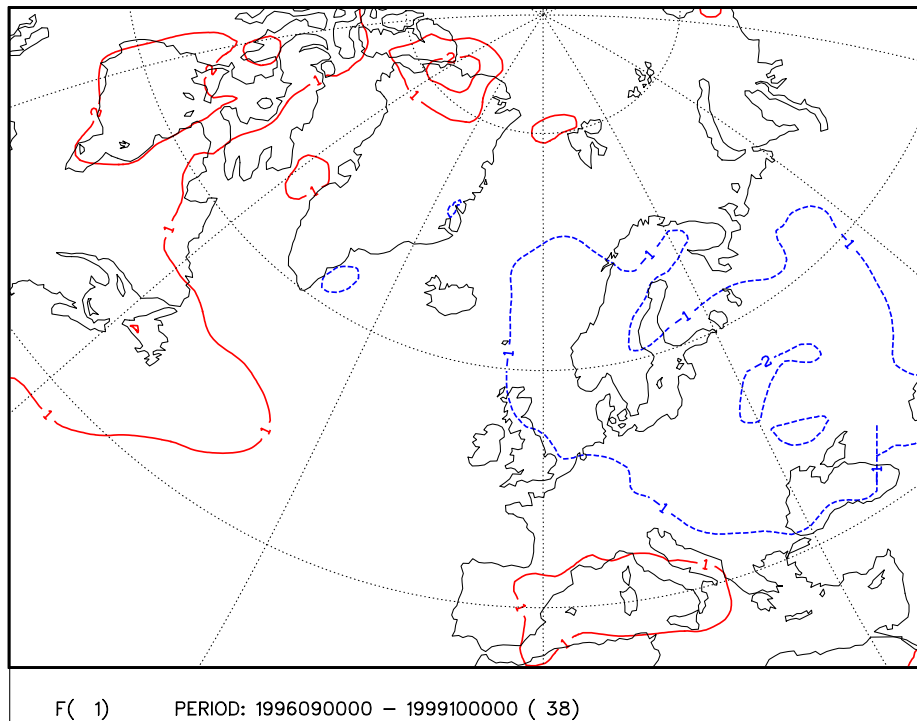


Figure 7: EOF-1 of the "LOU" 48 h monthly  $p_{msl}$  forecast error for September 1996 - October 1999. EOF-1 explains 47 % of the total forecast error variance. Contour interval: 1.0. The zero isoline not plotted, negative values indicated with dashed lines.

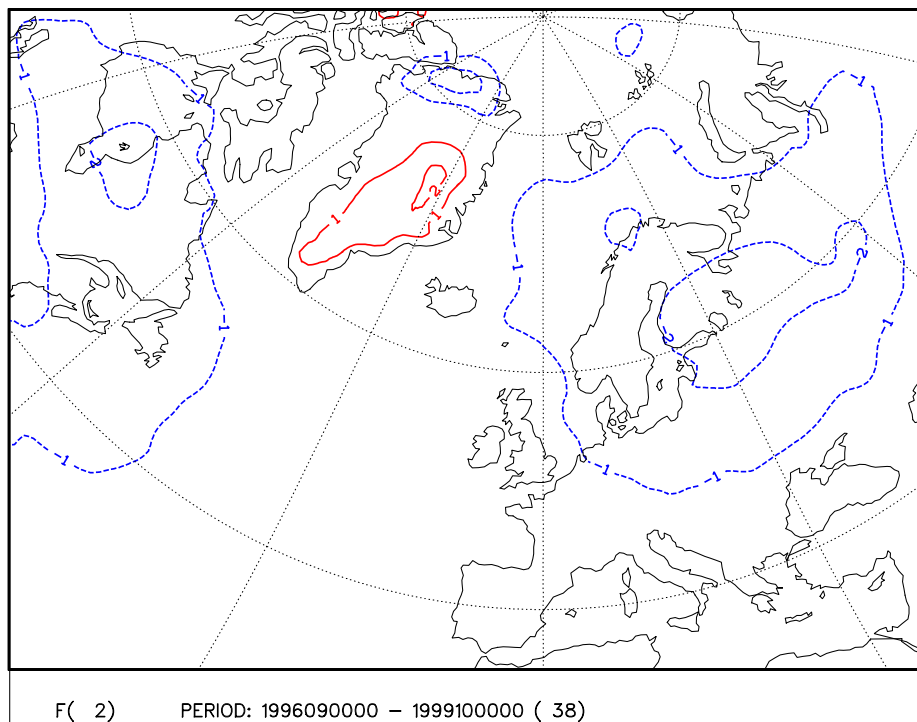


Figure 8: EOF-2 of the "LOU" 48 h monthly  $p_{msl}$  forecast error for September 1996 - October 1999. EOF-2 explains 10 % of the total forecast error variance. Contour interval: 1.0. The zero isoline not plotted, negative values indicated with dashed lines.

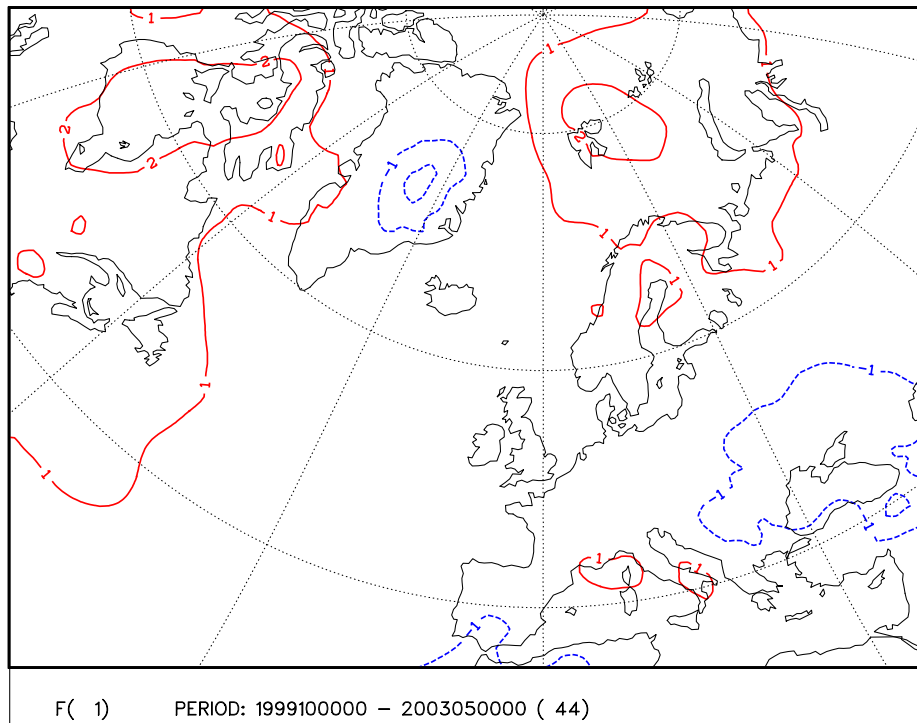


Figure 9: EOF-1 of the "CBR" 48 h monthly  $p_{msl}$  forecast error for October 1999 - May 2003. EOF-1 explains 49 % of the total forecast error variance. Contour interval: 1.0. The zero isoline not plotted, negative values indicated with dashed lines.

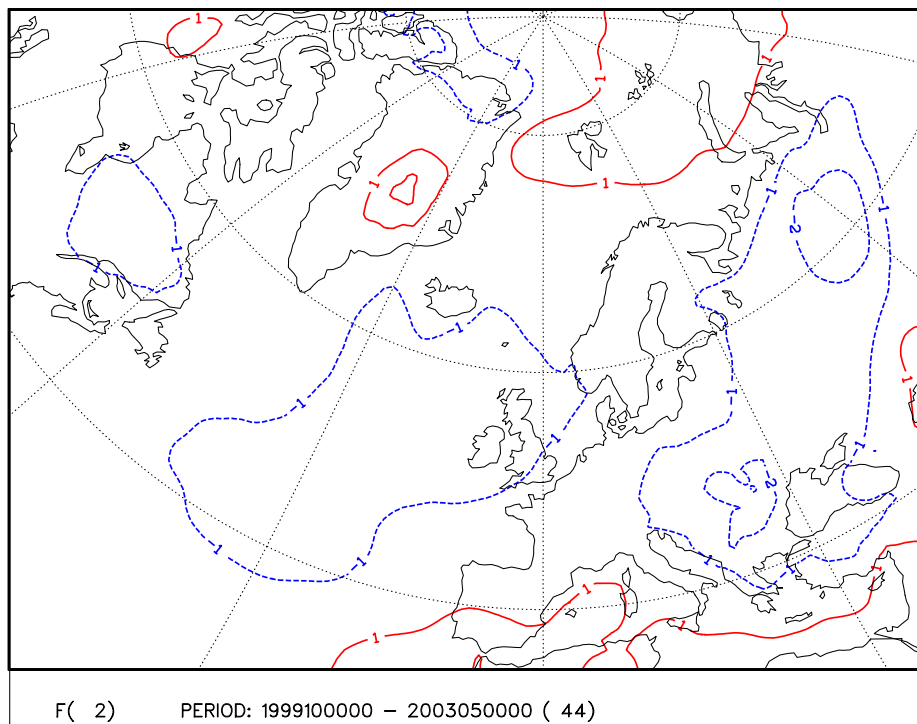


Figure 10: EOF-2 of the "CBR" 48 h monthly  $p_{msl}$  forecast error for October 1999 - May 2003. EOF-2 explains 8 % of the total forecast error variance. Contour interval: 1.0. The zero isoline not plotted, negative values indicated with dashed lines.

**Coefficients C1 and C2 for monthly Pmsl bias, Sep 1996 - May 2003**

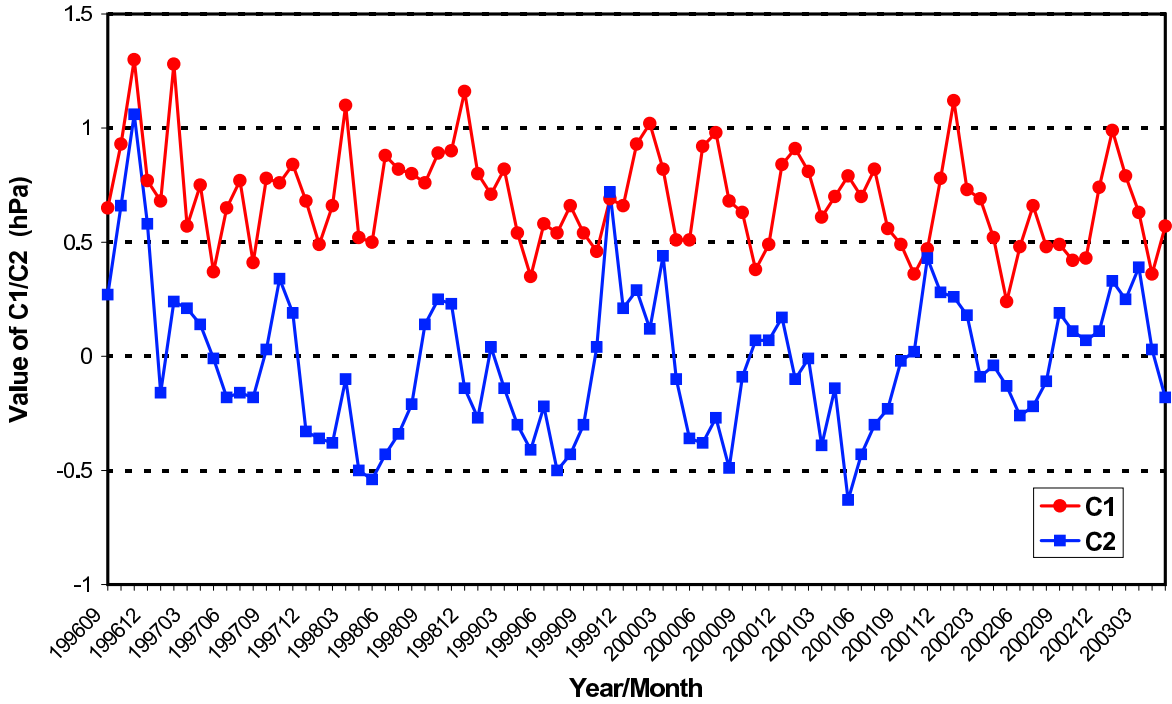


Figure 11: Time-dependent (monthly) coefficients  $C_1$  and  $C_2$ , for September 1996 - May 2003. Coefficients  $C_1$  correspond the spatial EOF-1 patterns of Figs. 7 and 9 and  $C_2$  spatial EOF-2 patterns of Figs. 8 and 10, in respective time periods.  $C_1$  is indicated with circles and  $C_2$  with squares.

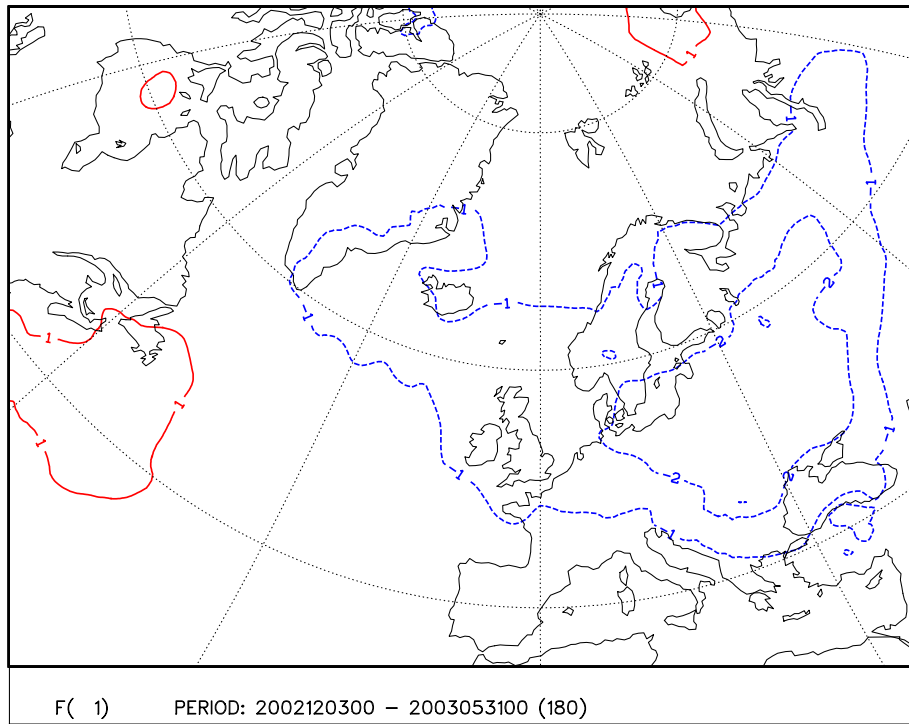


Figure 12: EOF-1 of the "CBN" 48 h daily  $p_{msl}$  forecast error for December 2002 - May 2003. EOF-1 explains 15 % of the total forecast error variance. Contour interval: 1.0. The zero isoline not plotted, negative values indicated with dashed lines.

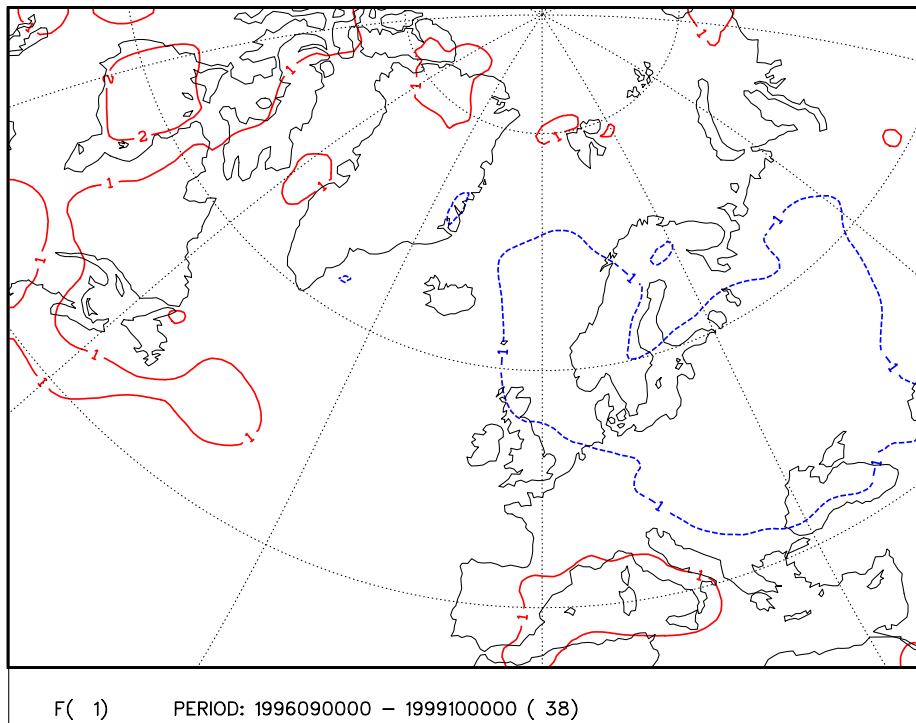


Figure 13: The forecast error part of CEOF-1 for the combined 48 h monthly  $p_{msl}$  forecast error and monthly  $p_{msl}$  departure of "LOU" period, September 1996 - October 1999. CEOF-1 explains 44 % of the total forecast error variance. Contour interval: 1.0. The zero isoline not plotted, negative values indicated with dashed lines.

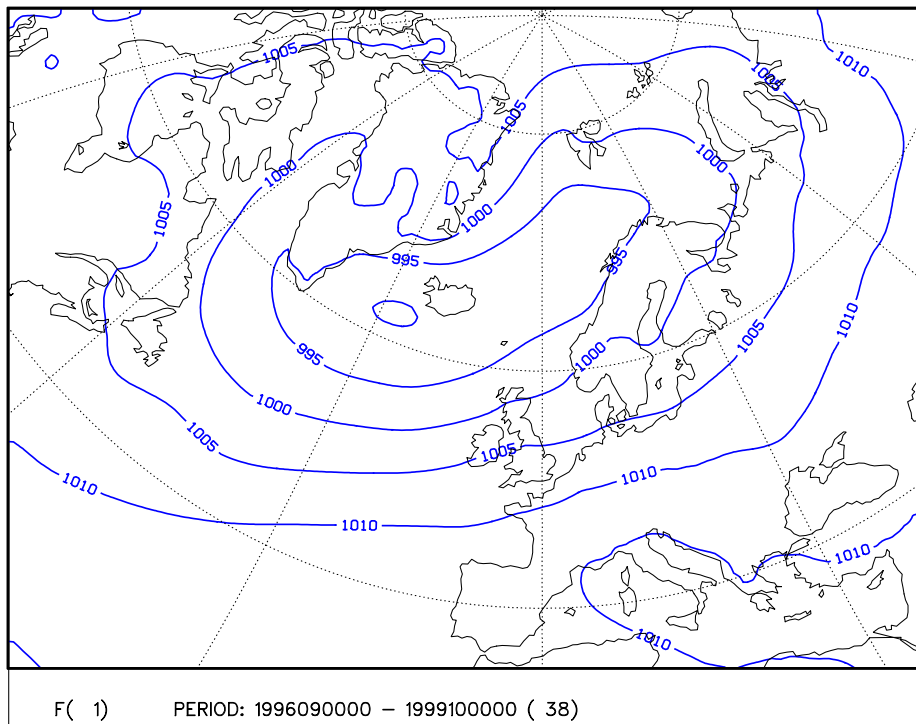


Figure 14: The departure part of CEOF-1 for the combined 48 h monthly  $p_{msl}$  forecast error and monthly  $p_{msl}$  departure of "LOU" period, September 1996 - October 1999. CEOF-1 explains 44 % of the total forecast error variance. The departure is expressed as a  $p_{msl}$  field (departure + average  $p_{msl}$ , see text). Contour interval: 5 hPa.

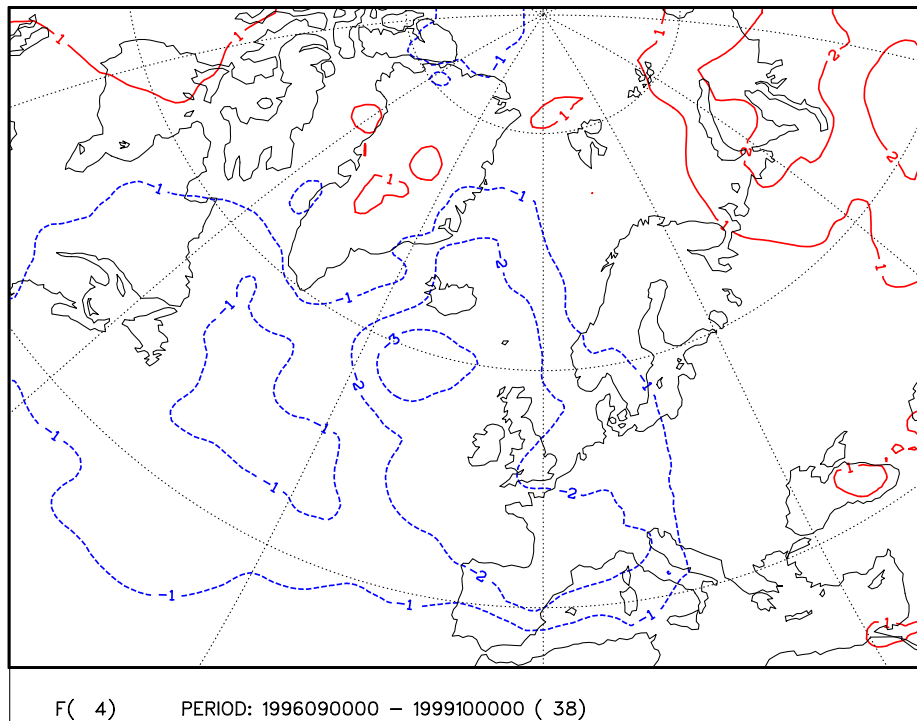


Figure 15: The forecast error part of CEOF-4 for the combined 48 h monthly  $p_{msl}$  forecast error and monthly  $p_{msl}$  departure of "LOU" period, September 1996 - October 1999. CEOF-4 explains 4 % of the total forecast error variance. Contour interval: 1.0. The zero isoline not plotted, negative values indicated with dashed lines.

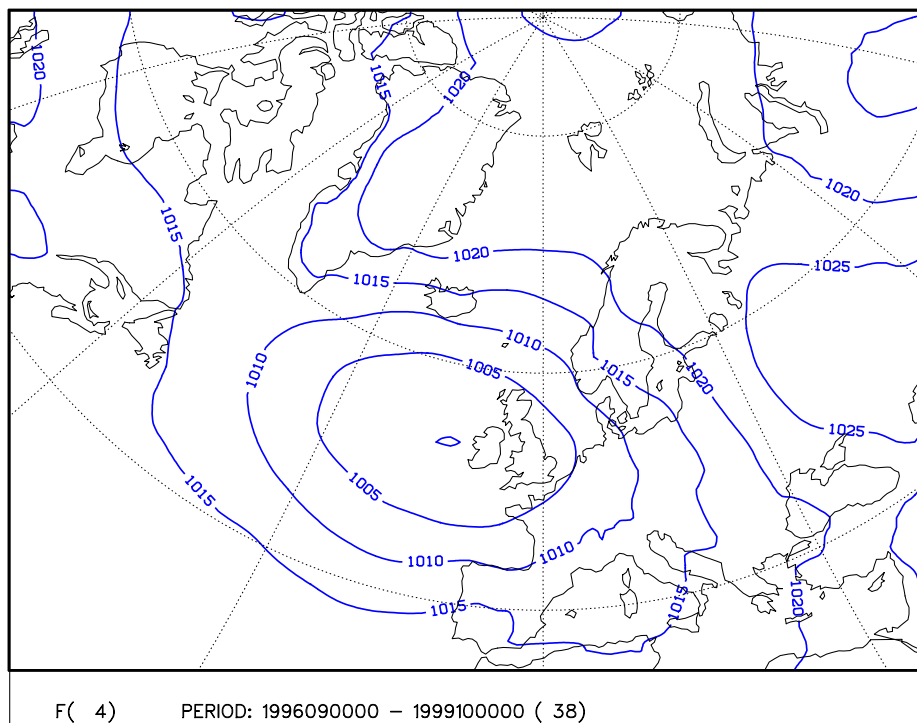


Figure 16: The departure part of CEOF-4 for the combined 48 h monthly  $p_{msl}$  forecast error and monthly  $p_{msl}$  departure of "LOU" period, September 1996 - October 1999. CEOF-4 explains 4 % of the total forecast error variance. The departure is expressed as a  $p_{msl}$  field (departure + average  $p_{msl}$ , see text). Contour interval: 5 hPa.

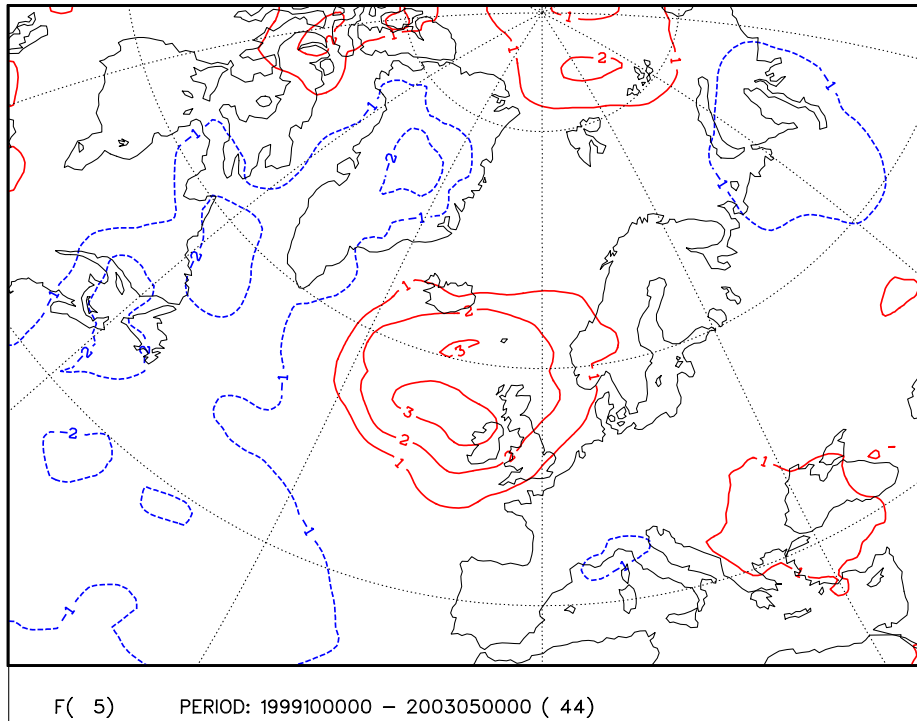


Figure 17: The forecast error part of CEOF-5 for the combined 48 h monthly  $p_{msl}$  forecast error and monthly  $p_{msl}$  departure of "CBR" period, October 1999 - May 2003. CEOF-5 explains 3 % of the total forecast error variance. Contour interval: 1.0. The zero isoline not plotted, negative values indicated with dashed lines.

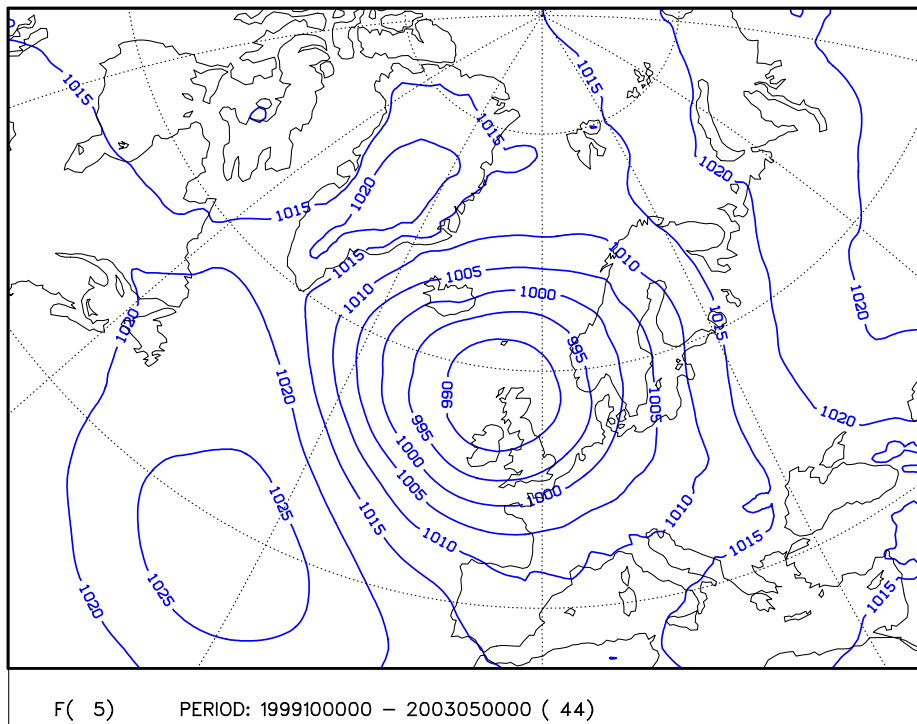


Figure 18: The departure part of CEOF-5 for the combined 48 h monthly  $p_{msl}$  forecast error and monthly  $p_{msl}$  departure of "LOU" period, October 1999 - May 2003. CEOF-5 explains 3 % of the total forecast error variance. The departure is expressed as a  $p_{msl}$  field (departure + average  $p_{msl}$ , see text). Contour interval: 5 hPa.

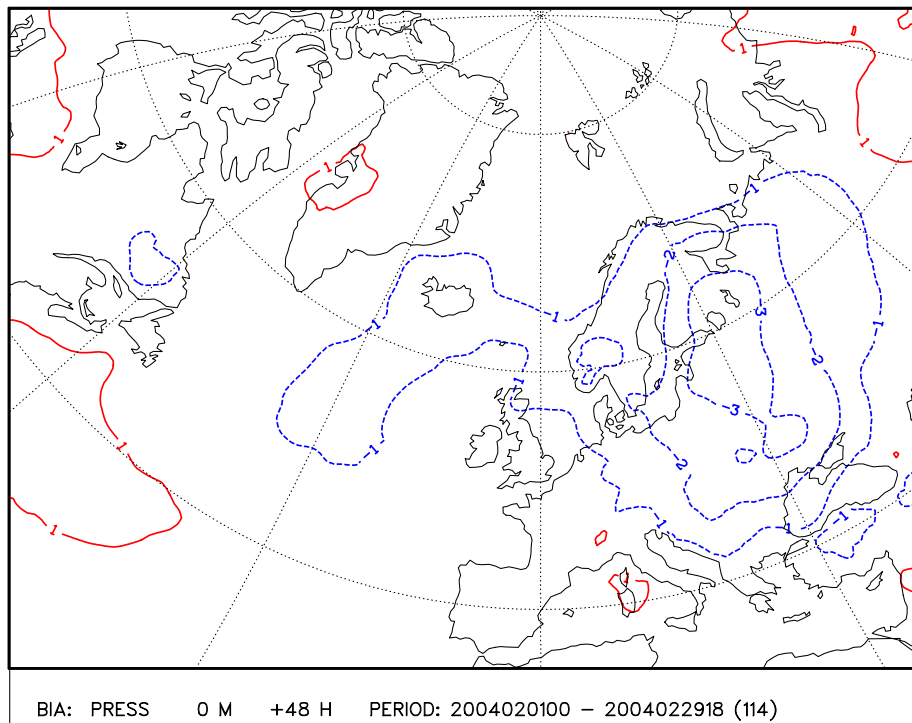


Figure 19: Bias of  $p_{msl}$  in ATX 48 h forecasts for February 2004. Contour interval: 1 hPa; the zero isoline not plotted, negative values indicated with dashed lines.

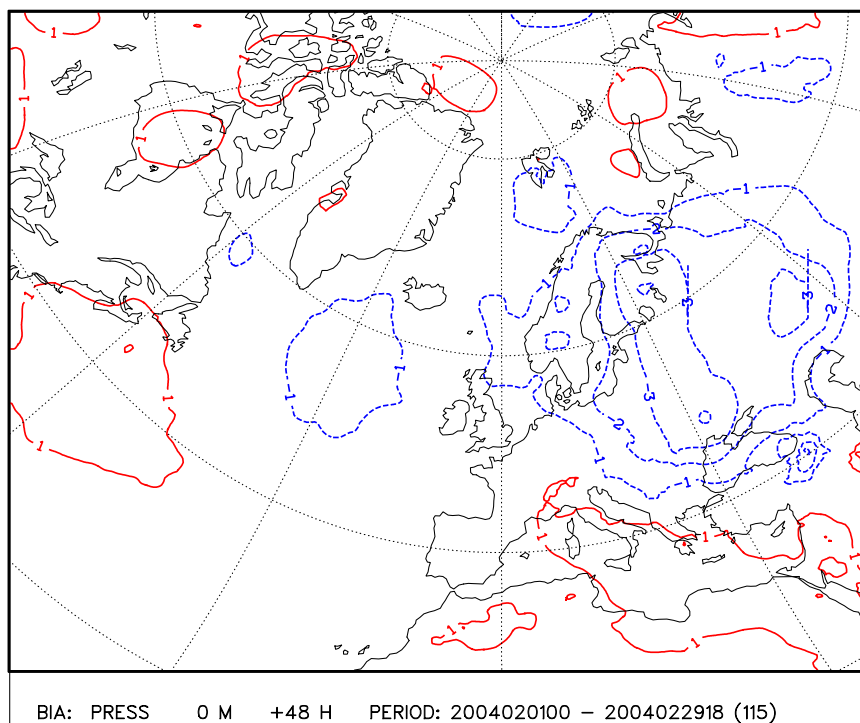


Figure 20: Bias of  $p_{msl}$  in RCR (V621) 48 h forecasts for February 2004. Contour interval: 1 hPa; the zero isoline not plotted, negative values indicated with dashed lines.